SAPIENZA
UNIVERSITÀ DI ROMA

TOR VERGATA
UNIVERSITÀ DEGLI STUDI DI ROMA

# Spectral imaging and pressure profiles of the X-COP galaxy clusters with the Sunyaev-Zel'dovich effect

Anna Silvia Baldi

Collaborators: H. Bourdin, P. Mazzotta & X-COP Collaboration

mm Universe @ NIKA2

Grenoble, 4 June 2019

# Outline

- **Introduction**
- **Imaging of the thermal Sunyaev–Zel'dovich effect**
  - Method: (improved) spectral imaging algorithm
  - Results for the X-COP clusters
- **Pressure profiles**
  - Recipe for unbiased profiles
  - Preliminary results for the X-COP clusters
- **Conclusions & future perspectives**

# The outskirts of galaxy clusters

They "mark the transition from the cosmic web to the ICM" (Avestruz et al., 2016).

Radial range of interest: $R_{500} < r < 3R_{200} \approx 3R_{\rm vir}$

## Outskirts dynamics

Accretion and gravity-driven processes that lead to:

- inhomogeneities in the ICM (substructures, clumps)
- shocks injecting turbulence
- filaments or bridges connecting objects

(see e.g. Vazza et al., 2013; Roncarelli et al., 2013; Reiprich et al., 2013; Avestruz et al., 2015; Walker et al., 2019)

↓

biases in the thermodynamic profiles and in the inferred cosmological quantities

# The XMM Cluster Outskirts Project

## Purpose

Study of the properties of galaxy cluster outskirts exploiting the synergy between X-ray and Sunyaev–Zel'dovich data (Eckert et al., 2017)

## Data set

Twelve massive galaxy clusters observed by *Planck* and *XMM-Newton*.
Selection criteria:

- significant *Planck* detection: SNR $> 12$
- low redshift: $0.04 < z < 0.10$
- objects well resolved by *Planck*: $\theta_{500} > 10$ arcmin

## Significant update

In this work we make use of the *Planck* 2018 data release (PR3)

(available at `https://pla.esac.esa.int`)

# *Planck* data

*Planck* data for cluster science are collected by the High Frequency Instrument (HFI) (Planck Collaboration et al., 2014; Planck Collaboration et al., 2018)

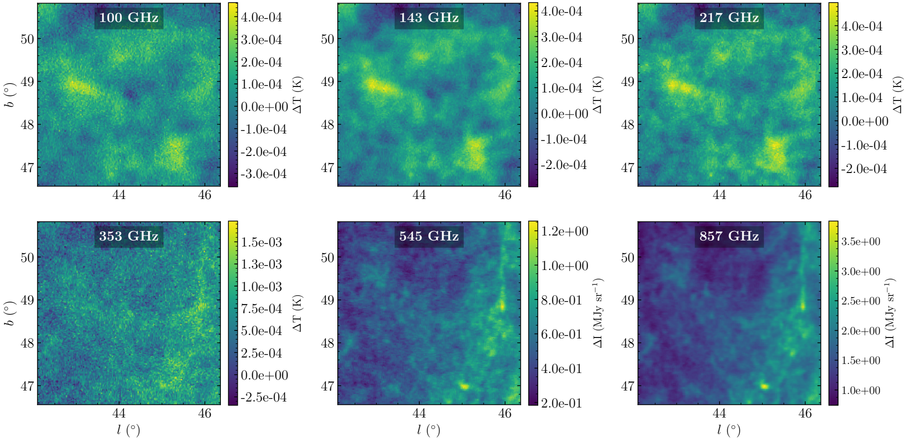


Raw maps from PR3 centred on cluster A2142

# Thermal Sunyaev–Zel'dovich effect

Spectral distortion of the cosmic microwave background from inverse Compton scattering with the free electrons in the ICM (Sunyaev & Zel'dovich, 1970).

Shift for $x = \frac{k_B T_{\rm CMB}}{m_e c^2} \ll 1$ (Kompaneets, 1957):

$$\frac{\Delta T_{\rm tSZ}}{T_{\rm CMB}} = f(x)\; y \qquad \frac{\Delta I_{\rm tSZ}}{I_{\rm CMB}} = g(x)\; y$$

For a thermal population of electrons: ➔

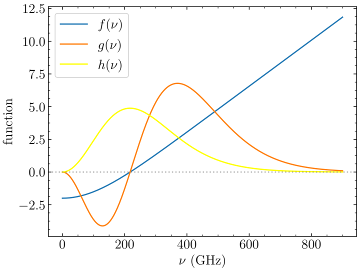


Definition of the Compton $y$ parameter:

$$y = \frac{\sigma_T}{m_e c^2} \int_{\rm los} p_e(l)\; dl$$

...direct probe of the ICM pressure along the line of sight

# Cluster imaging with the tSZ effect

## The problem of component separation

Different methods used in mm astronomy, e.g.:

- internal linear combination methods;
- blind or semi-blind methods based on spatial modelling;
- parametric methods

# Cluster imaging with the tSZ effect

## The problem of component separation

Different methods used in mm astronomy, e.g.:

- internal linear combination methods;
- blind or semi-blind methods based on spatial modelling;
- parametric methods

## Our spectral imaging

We propose an improved version of the algorithm presented in **Bourdin et al. (2015)** (B15), applied for the first time to *Planck* 2018 data.

It aims at combining:

- the robustness of parametric component separation
- the advantages offered by sparse representations to map localized features (use of wavelet and curvelet transforms)

# Basics of B15 algorithm: the parametric way

Temperature anisotropies in HFI data can be modelled at each frequency $\nu$ as:

$$M(\nu, k; s) = \sum_{i}^{N_s} f_i(\nu)\ s_i(k) + \eta(\nu, k)$$

$k$: generic pixel in the maps.

**Ingredients of the model maps**

- $f_i$: spectral energy density
- $s_i$: signal from each component
- $N_s$: total number of components
- $\eta$: instrumental noise

Only three dominating sources: CMB, Galactic thermal dust and tSZ

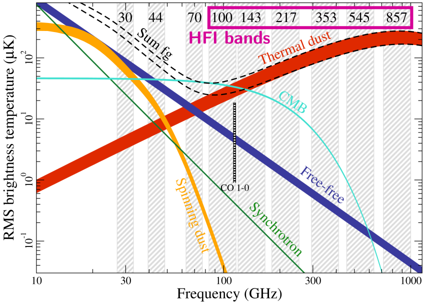


(Planck Collaboration et al., 2016)

The component maps are estimated from a chi-square minimization.

# Basics of B15 algorithm: the parametric way

Temperature anisotropies in HFI data can be modelled at each frequency $\nu$ as:

$$M(\nu, k; s) = \sum_{i}^{N_s} f_i(\nu)\; s_i(k) + \eta(\nu, k)$$

$k$: generic pixel in the maps.

**Ingredients of the model maps**

- $f_i$: spectral energy density
- $s_i$: signal from each component
- $N_s$: total number of components
- $\eta$: instrumental noise

Only three dominating sources: CMB, Galactic thermal dust and tSZ

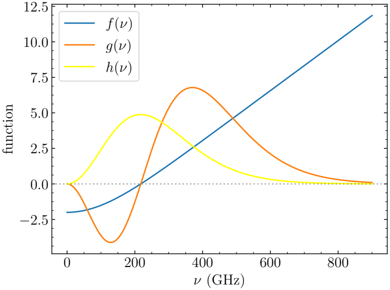


. . . plus thermal SZ

The component maps are estimated from a chi-square minimization.

# Basics of B15 algorithm: the sparse way

We introduce sparsity in the chi-square by implementing a wavelet decomposition of the residuals between the data, $D_{\rm HFI}$, and the model $M$:

$$\mathrm{res}(\nu, k; s) = D_{\rm HFI}(\nu, k) - M(\nu, k; s)$$

Their wavelet transform is (e.g. Mallat, 2008):

$$\mathrm{res}_{\Psi}(\nu, k; s) = \sum_{n}^{N_{\rm pix}} a_{j_0,n}(\nu; s)\ \Phi_{j_0,n}(k) + \sum_{j=j_0}^{N_{\rm scales}} \sum_{n}^{N_{\rm pix}} a_{j,n}(\nu; s)\ \Psi_{j,n}(k)$$

# Basics of B15 algorithm: the sparse way

We introduce sparsity in the chi-square by implementing a wavelet decomposition of the residuals between the data, $D_{\mathrm{HFI}}$, and the model $M$:

$$\mathrm{res}(\nu, k; s) = D_{\mathrm{HFI}}(\nu, k) - M(\nu, k; s)$$

Their wavelet transform is (e.g. Mallat, 2008):

$$\mathrm{res}_{\Psi}(\nu, k; s) = \sum_{n}^{N_{\mathrm{pix}}} a_{j_0,n}(\nu; s)\ \Phi_{j_0,n}(k) + \sum_{j=j_0}^{N_{\mathrm{scales}}} \sum_{n}^{N_{\mathrm{pix}}} a_{j,n}(\nu; s)\ \Psi_{j,n}(k)$$

approximation coefficients:

$$a_{j_0,n}(\nu; s) = \sum_{m}^{N_{\mathrm{pix}}} \mathrm{res}(\nu, m; s)\ \Phi^{*}_{j_0,n}(m)$$

detail coefficients:

$$a_{j,n}(\nu; s) = \sum_{m}^{N_{\mathrm{pix}}} \mathrm{res}(\nu, m; s)\ \Psi^{*}_{j,n}(m)$$

$\Phi$: dual scaling function of $\Psi$ at the scale $j_0$

$\Psi$: $\mathrm{B}_3$ spline wavelet

# Basics of B15 algorithm: the sparse way

In order to ensure positivity and unity normalization, the kernel (and its dual) are split into its positive and negative components:

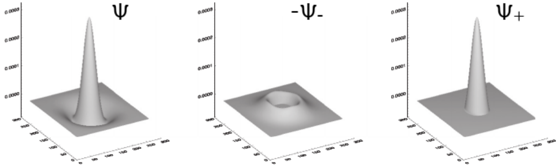


And the best-fit source component maps are estimated by:

$$\hat{s} = \frac{1}{2}\left[\underset{s}{\mathrm{argmin}}(\chi^2_{\Psi_+}) - \underset{s}{\mathrm{argmin}}(\chi^2_{\Psi_-})\right]$$

being the weighted chi-squares:

$$\chi^2_{\Psi_\pm} = \sum_{\nu}^{N_\nu} \sum_{k}^{N_{\mathrm{pix}}} \frac{\mathrm{res}^2_{\Psi_\pm}(k,\nu;s)}{\sigma^2_{\mathrm{HFI}}(k,\nu)}$$

# Basics of B15 algorithm: the sparse way

In order to ensure positivity and unity normalization, the kernel (and its dual) are split into its positive and negative components:

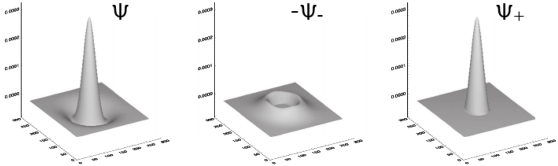


And the best-fit source component maps are estimated by:

$$\hat{s} = \frac{1}{2}\left[\underset{s}{\mathrm{argmin}}(\chi^2_{\Psi_+}) - \underset{s}{\mathrm{argmin}}(\chi^2_{\Psi_-})\right]$$

being the weighted chi-squares: ➔ deconvolution needed!

$$\chi^2_{\Psi_\pm} = \sum_{\nu}^{N_\nu} \sum_{k}^{N_{\mathrm{pix}}} \frac{\mathrm{res}^2_{\Psi_\pm}(k,\nu;s)}{\sigma^2_{\mathrm{HFI}}(k,\nu)}$$

# Enhancement of B15 algorithm: new deconvolution

The new deconvolution is applied directly to the wavelet coefficients of the residuals, which we rewrite as:

$$a_{j,n}(\nu;\Delta s) = \sum_{m}^{N_{\rm pix}} \{ D_{\rm HFI}(\nu,k) - B(\nu) \otimes [HM(\nu,m;\tilde{s}+\Delta s) + \\ + (1-H)M(\nu,m;\tilde{s}-\Delta s)]\} \, \Psi^{*}_{j,n}(m)$$

$B(\nu)$: instrumental beam; $H$: Heaviside step function; $s = \tilde{s} \pm \Delta s$

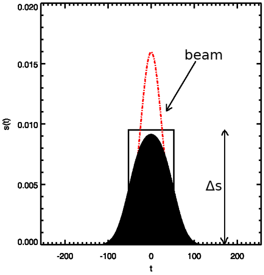


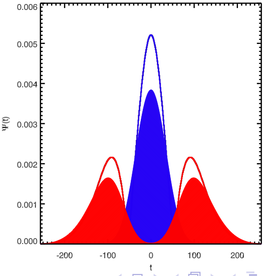

# Overall enhancement of B15 algorithm

## Improvements and new features

Major change to improve the performance and the stability of the algorithm:

Adaptation to real cluster observations:

(Baldi et al., to be submitted)

# Overall enhancement of B15 algorithm

## Improvements and new features

Major change to improve the performance and the stability of the algorithm:

- the former iterative deconvolution has been replaced with the new *wavelet coefficient-wise* deconvolution shown before

Adaptation to real cluster observations:

(Baldi et al., to be submitted)

# Overall enhancement of B15 algorithm

## Improvements and new features

Major change to improve the performance and the stability of the algorithm:

- the former iterative deconvolution has been replaced with the new *wavelet coefficient-wise* deconvolution shown before

Adaptation to real cluster observations:

- an updated model of thermal dust ➔ two grey bodies as in Meisner & Finkbeiner (2015):

$$f_{\mathrm{td}}(\nu) = f_1 \frac{q_1}{q_2} \left( \frac{\nu}{\nu_0} \right)^{\beta_1} B(\nu; T_1) + (1 - f_1) \left( \frac{\nu}{\nu_0} \right)^{\beta_2} B(\nu; T_2)$$

(Baldi et al., to be submitted)

# Overall enhancement of B15 algorithm

## Improvements and new features

Major change to improve the performance and the stability of the algorithm:

- the former iterative deconvolution has been replaced with the new *wavelet coefficient-wise* deconvolution shown before

Adaptation to real cluster observations:

- an updated model of thermal dust ➔ two grey bodies as in Meisner & Finkbeiner (2015):

$$f_{\rm td}(\nu) = f_1 \frac{q_1}{q_2} \left(\frac{\nu}{\nu_0}\right)^{\beta_1} B(\nu; T_1) + (1 - f_1) \left(\frac{\nu}{\nu_0}\right)^{\beta_2} B(\nu; T_2)$$

- removal of residual contamination from:

(Baldi et al., to be submitted)

# Overall enhancement of B15 algorithm

## Improvements and new features

Major change to improve the performance and the stability of the algorithm:

- the former iterative deconvolution has been replaced with the new *wavelet coefficient-wise* deconvolution shown before

Adaptation to real cluster observations:

- an updated model of thermal dust ➔ two grey bodies as in Meisner & Finkbeiner (2015):

$$f_{\rm td}(\nu) = f_1 \frac{q_1}{q_2} \left(\frac{\nu}{\nu_0}\right)^{\beta_1} B(\nu; T_1) + (1 - f_1) \left(\frac{\nu}{\nu_0}\right)^{\beta_2} B(\nu; T_2)$$

- removal of residual contamination from:
  - dust ➔ 857 GHz channel not used in the approximation coefficients

(Baldi et al., to be submitted)

# Overall enhancement of B15 algorithm

## Improvements and new features

Major change to improve the performance and the stability of the algorithm:

- the former iterative deconvolution has been replaced with the new *wavelet coefficient-wise* deconvolution shown before

Adaptation to real cluster observations:

- an updated model of thermal dust ➔ two grey bodies as in Meisner & Finkbeiner (2015):

$$f_{\rm td}(\nu) = f_1 \frac{q_1}{q_2} \left(\frac{\nu}{\nu_0}\right)^{\beta_1} B(\nu; T_1) + (1 - f_1) \left(\frac{\nu}{\nu_0}\right)^{\beta_2} B(\nu; T_2)$$

- removal of residual contamination from:
  - dust ➔ 857 GHz channel not used in the approximation coefficients
  - bright point sources ➔ masking with the Planck Catalogue of Compact Sources (Planck Collaboration et al., 2014, 2016)

(Baldi et al., to be submitted)

# TSZ maps of the X-COP clusters

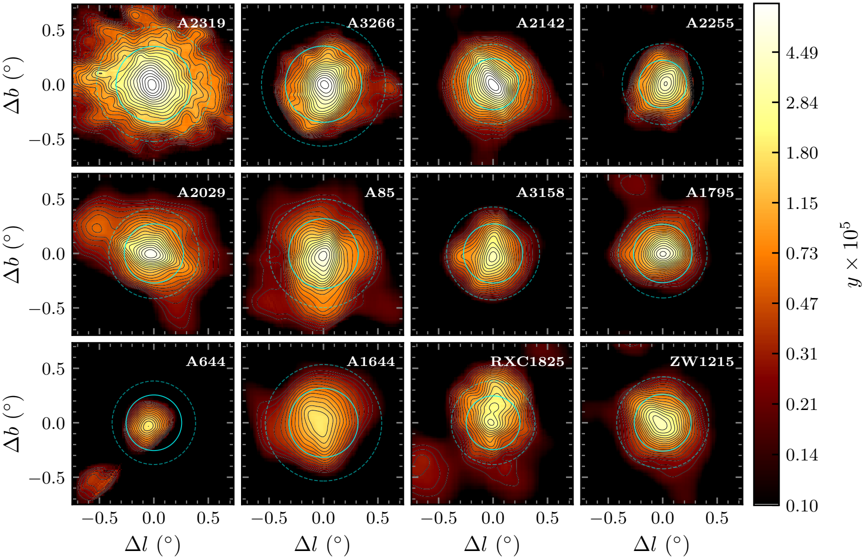


(Baldi et al., to be submitted)

# A2029: tSZ + X-ray (*ROSAT*/PSPC)

cyan cross: cluster A2033

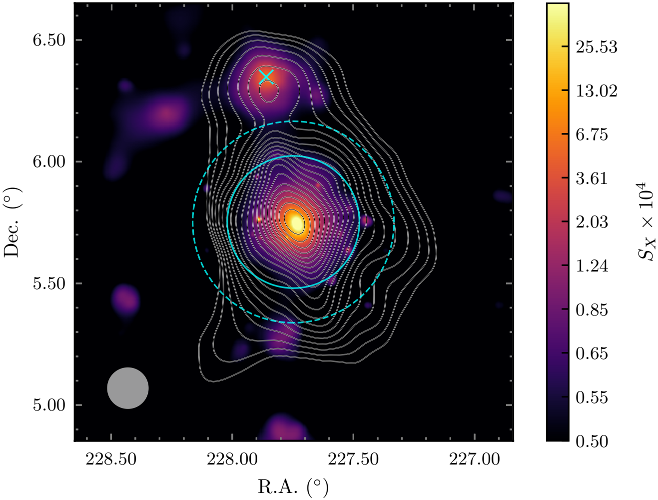


(Baldi et al., to be submitted)

# RXC1825: tSZ + X-ray (*XMM-Newton*)

cyan cross: cluster CIZA1824

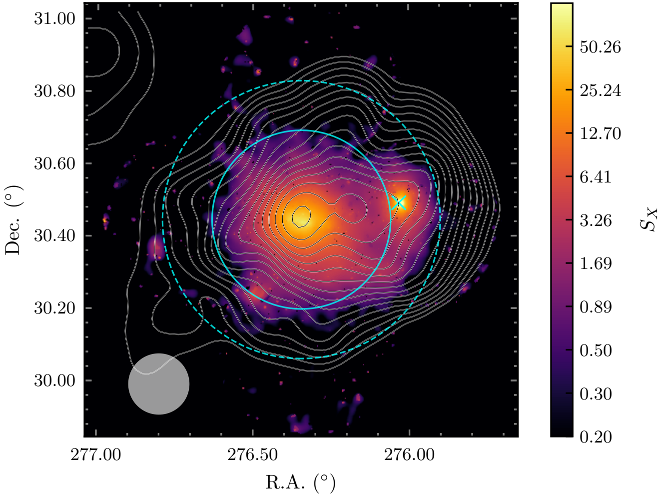


(Baldi et al., to be submitted)

# Additional step: error estimate

## Bootstrap technique to get mock HFI data

Three steps:

# Additional step: error estimate

## Bootstrap technique to get mock HFI data

Three steps:

1. denoising of the HFI raw frequency maps through a simple wavelet transform with $1.5\sigma$ thresholding ➔ $D_{\mathrm{HFI,den}}(\nu)$

# Additional step: error estimate

## Bootstrap technique to get mock HFI data

Three steps:

1. denoising of the HFI raw frequency maps through a simple wavelet transform with $1.5\sigma$ thresholding ➔ $D_{\mathrm{HFI,den}}(\nu)$
2. generation of $N_{\mathrm{tot}} = 100$ noise realizations from *Planck* jackknife maps of the sky region of interest ➔ $\eta_u(\nu)$ $(u = 1, \ldots, N_{\mathrm{tot}})$

# Additional step: error estimate

## Bootstrap technique to get mock HFI data

Three steps:

1. denoising of the HFI raw frequency maps through a simple wavelet transform with $1.5\sigma$ thresholding ➔ $\boxed{D_{\mathrm{HFI,den}}(\nu)}$
2. generation of $N_{\mathrm{tot}} = 100$ noise realizations from *Planck* jackknife maps of the sky region of interest ➔ $\boxed{\eta_u(\nu)}$ $(u = 1, \ldots, N_{\mathrm{tot}})$
3. calculation of the $N_{\mathrm{tot}}$ simulated frequency maps ➔

$$\boxed{D_{\mathrm{HFI}\,u}(\nu) = D_{\mathrm{HFI,den}}(\nu) + \eta_u(\nu)}$$

# Additional step: error estimate

## Bootstrap technique to get mock HFI data

Three steps:

1. denoising of the HFI raw frequency maps through a simple wavelet transform with $1.5\sigma$ thresholding ➔ $D_{\mathrm{HFI,den}}(\nu)$
2. generation of $N_{\mathrm{tot}} = 100$ noise realizations from *Planck* jackknife maps of the sky region of interest ➔ $\eta_u(\nu)$ $(u = 1, \ldots, N_{\mathrm{tot}})$
3. calculation of the $N_{\mathrm{tot}}$ simulated frequency maps ➔

$$D_{\mathrm{HFI}\,u}(\nu) = D_{\mathrm{HFI,den}}(\nu) + \eta_u(\nu)$$

## Error maps

$D_{\mathrm{HFI}\,u}(\nu)$ ➔ imaging algorithm ➔ $s_{\mathrm{tSZ}\,u}$

We set the tSZ error to be $\sigma_d = \mathrm{std}(s^1_{\mathrm{tSZ}}, \ldots, s^{N_{\mathrm{tot}}}_{\mathrm{tSZ}})$

(Baldi et al., to be submitted)

# Significance of the signal: $y/\sigma_d$

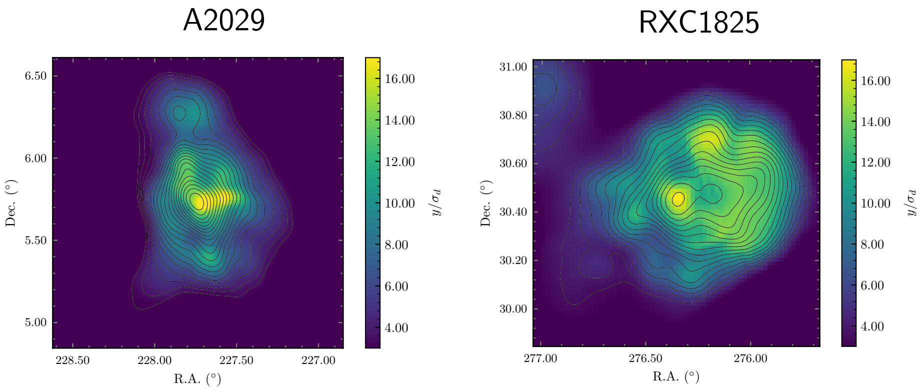


TSZ contours overlaid

Minimum value shown in the maps: $y/\sigma_d \geq 3$

Signal detected for all clusters at this minimum significance

(Baldi et al., to be submitted)

# A comparison with B15 version: cluster A2319

## Maps of the tSZ effect

B15 version

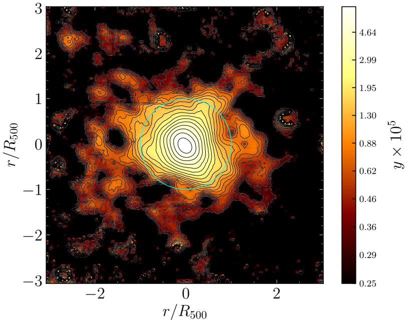


New version

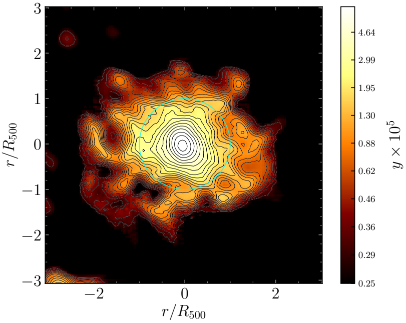


Main differences:

- effect of removing the 857 GHz channel from last smooth
- impact of the new deconvolution

(Baldi et al., to be submitted)

# A comparison with B15 version: cluster A2319

## Cuts from bootstrap maps

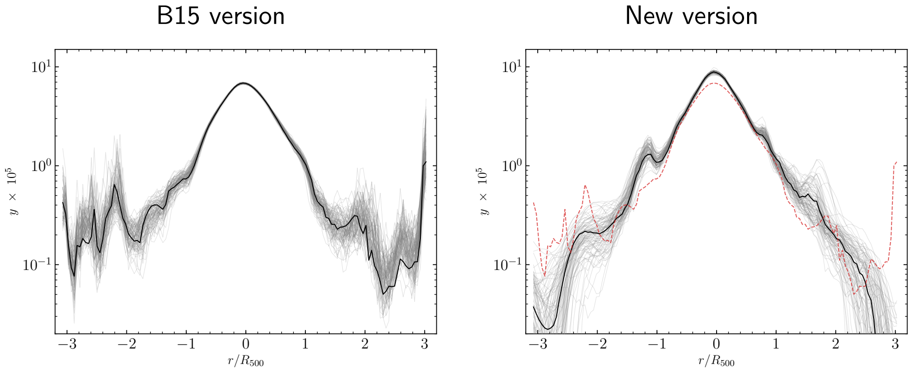


Main differences:

- effect of removing the 857 GHz channel from last smooth
- impact of the new deconvolution ➔ reliable reconstruction down to $y \approx 10^{-6}$

(Baldi et al., to be submitted)

# Substructures vs pressure profiles

## Using the tSZ for detecting overpressure

NIKA and NIKA2 already shed some light on this, see:

- Adam et al. (2018): promising results from the application of filtering techniques
- Ruppin et al. (2018): assessment of substructure impact on the pressure profile and mass estimate of cluster PSZ2 G144.83+25.11
- Ruppin et al. (2019): pressure profiles vs cluster morphology of twin clusters between MUSIC2 and NIKA2 tSZ Large Program

## NIKA2 vs *Planck*

- NIKA2's high angular resolution and sensitivity makes it suitable for intermediate to high redshift clusters
- *Planck*, on the other hand, allows the investigation of large and nearby objects ➔ X-COP

# Masks for unbiased pressure profiles

**Proposed method**

Three steps:

# Masks for unbiased pressure profiles

## Proposed method

Three steps:

1. use our tSZ maps to identify substructures

# Masks for unbiased pressure profiles

## Proposed method

Three steps:

1. use our tSZ maps to identify substructures
2. mask the corresponding pixels in the HFI maps

# Masks for unbiased pressure profiles

## Proposed method

Three steps:

1. use our tSZ maps to identify substructures
2. mask the corresponding pixels in the HFI maps
3. extract cluster pressure profiles (*forward approach* of Bourdin et al., 2017)

# Masks for unbiased pressure profiles

## Proposed method

Three steps:

1. use our tSZ maps to identify substructures
2. mask the corresponding pixels in the HFI maps
3. extract cluster pressure profiles (*forward approach* of Bourdin et al., 2017)

## Conditions imposed for masking

The overpressure signal from substructures is identified as:

$$y_{\rm subs} = y - y_{\rm model} \quad \text{and} \quad y_{\rm subs} > y_{\rm bck}$$

being:

- $y$: total ySZ map, renormalized to $y_{\rm model}$
- $y_{\rm model}$: model map (NKV07 with the parameters from the best fit)
- $y_{\rm bck}$: background signal estimated as $y_{\rm bck} = \langle y(r > 4R_{500}) \rangle$

# Masks for the X-COP clusters

(Preliminary!)

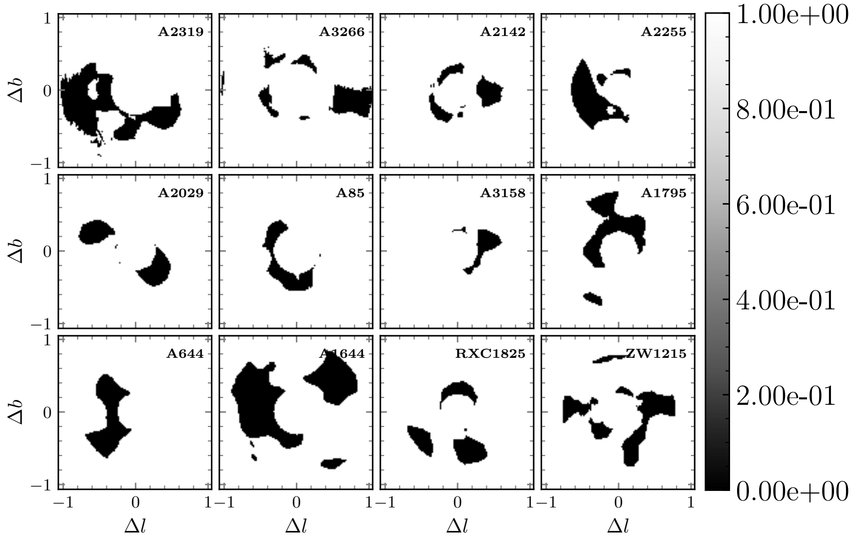

# Some examples: A2319

(Preliminary!)

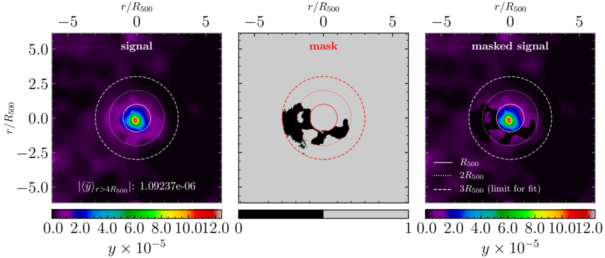


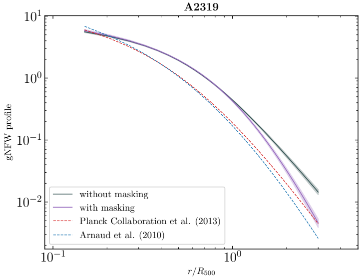

# Some examples: A2029

(Preliminary!)

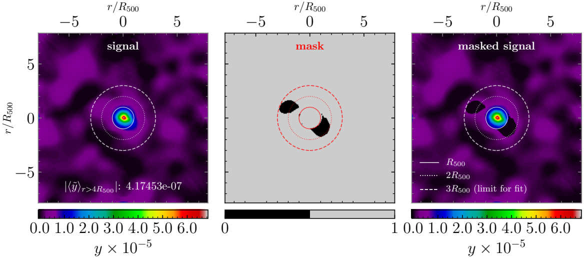


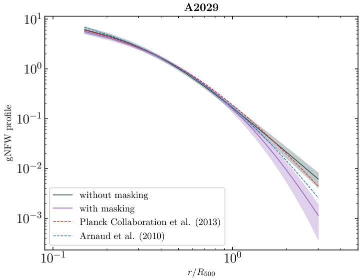

# Some examples: A1795

(Preliminary!)

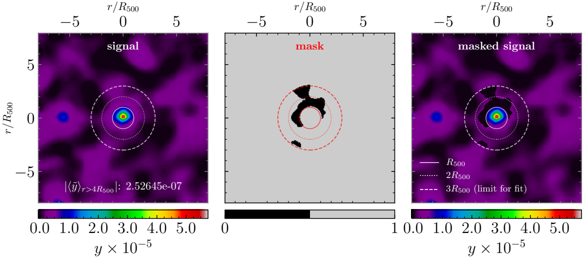


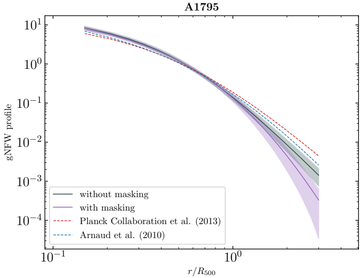

# Final remarks

## Conclusions

We presented:

- an improved parametric algorithm featuring sparse representations to map the tSZ effect, from *Planck* 2018 data for the X-COP clusters, showing:
  - capability of detecting anisotropic features in the outskirts down to $y \approx 1 \times 10^{-6}$ with high significance
  - agreement with known results from literature and ancillary X-ray data
- a possible method to estimate unbiased pressure profiles from the masking of tSZ-detected overpressure, finding promising preliminary results for the X-COP clusters

## Upcoming developments

- A detailed analysis of pressure profiles upgraded to *Planck* PR3 data
- a dedicated work on the most significant tSZ detection by *Planck*: A2319

. . . plus possible works to exploit the synergy with NIKA2 data for selected targets

# Thank you!